Advanced Composite Materials
Publication details, including instructions for authors and subscription information:
http://www.tandfonline.com/loi/tacm20

Influence of Biaxial Loads on Impact Fracture of High-Strength Membrane Materials

Hisashi Kumazawa [a], Ippei Susuki [b], Osamu Hasegawa [c] & Hideaki Kasano [d]

[a] Aerospace Research and Development Directorate, Japan Aerospace Exploration Agency 6-13-1 Ohsawa, Mitaka-shi, Tokyo, Japan, 181-0015;, Email: kumazawa.hisashi@jaxa.jp

[b] Aerospace Research and Development Directorate, Japan Aerospace Exploration Agency 6-13-1 Ohsawa, Mitaka-shi, Tokyo, Japan, 181-0015

[c] Department of Mechanical System Engineering, Takushoku University 815-1 Tatemachi, Hachioji-shi, Tokyo, Japan 193-0985

[d] Department of Mechanical System Engineering, Takushoku University 815-1 Tatemachi, Hachioji-shi, Tokyo, Japan 193-0985

Version of record first published: 02 Apr 2012.

To cite this article: Hisashi Kumazawa , Ippei Susuki , Osamu Hasegawa & Hideaki Kasano (2009): Influence of Biaxial Loads on Impact Fracture of High-Strength Membrane Materials, Advanced Composite Materials, 18:4, 395-413

To link to this article: http://dx.doi.org/10.1163/156855109X434793

VSP

Advanced Composite Materials 18 (2009) 395–413

ADVANCED COMPOSITE MATERIALS
www.brill.nl/acm

Influence of Biaxial Loads on Impact Fracture of High-Strength Membrane Materials

Hisashi Kumazawa [a,*], **Ippei Susuki** [a], **Osamu Hasegawa** [b] **and Hideaki Kasano** [b]

[a] Aerospace Research and Development Directorate, Japan Aerospace Exploration Agency 6-13-1 Ohsawa, Mitaka-shi, Tokyo, Japan, 181-0015

[b] Department of Mechanical System Engineering, Takushoku University 815-1 Tatemachi, Hachioji-shi, Tokyo, Japan 193-0985

Received 26 November 2008; accepted 2 December 2008

Abstract

Impact tests on high-strength membrane materials under biaxial loads were experimentally conducted in order to evaluate influence of biaxial loads on impact fracture of the membrane materials for the inflated applications. Cruciform specimens of the membrane materials were fabricated for applying biaxial loadings during the impact test. A steel ball was shot using a compressed nitrogen gas gun, and struck the membrane specimen. Impact tests on uniaxial strip specimens were also conducted to obtain the effect of specimen configuration and boundary condition on the impact fracture. The results of the measured crack length and the ultra-high speed photographs indicate the impact fracture properties of the membrane fabrics under biaxial loadings. Crack length due to the impact increased with applied tensile load, and the impact damages of the cruciform membrane materials under biaxial loadings were smaller than those of under uniaxial loadings. Impact fracture of the strip specimen was more severe than that of the cruciform specimen due to the difference of boundary conditions.

Keywords

Coated weave fabrics, impact fracture, biaxial load, cruciform specimen, high-speed photography

1. Introduction

High-performance flexible membrane materials composed of high-strength fibers such as polyarylate and PBO (poly-*p*-phenylenebenzobisoxazole) are being used in practical applications. Many of these membrane fabric materials are coated with polymer films to improve tolerance against ultraviolet radiation, moisture absorption and to provide airtightness. Several applications of flexible membranes are

* To whom correspondence should be addressed. E-mail: kumazawa.hisashi@jaxa.jp
Edited by JSCM

 DOI:10.1163/156855109X434793

planned in the field of aerospace structures. Stratospheric airships [1, 2] and deployable space structures [3] made from the membrane materials have been proposed. Applications with new structure configuration will be proposed through the use of the high-performance membrane materials.

The high-strength fabrics also have good impact resistance, and have already been applied to the manufacture of bullet-proof vests. These fabrics in the aerospace field have been applied to jet engine nacelles [4] to prevent penetration of fragments of fan blades. An installation of PBO fabrics in airplane fuselage walls was evaluated for protection from high-speed fragments of the fan blade, and high reliability for the impact resistance was achieved without large weight increase of the fuselage [5].

The good impact resistance of high-strength fabrics is put to practical use in the field of space exploration. Polyarylate fiber, VECTRAN (Kuraray Co. Ltd., Japan), plain weave fabrics evaluated in this study were applied to airbag landing systems of the Mars Exploration Program developed by the National Aeronautics and Space Administration (NASA) [7–9] and protectors in an asteroid sample capturing device of an unmanned spacecraft HAYABUSA developed by the Japan Aerospace Exploration Agency (JAXA) [6]. The Mars Exploration Rovers (Mars Path Finder in 1997, Opportunity and Spirit in 2004) successfully landed on Mars using the airbag system. In the development of the airbag system, tests of the full scale air bags system had been conducted repeatedly on simulated Martian terrain. The airbag system had been improved cumulatively in this series of tests, and finally the airbag structure was determined.

In addition to the full-scale structure tests mentioned above, small coupon tests were also conducted to experimentally clarify the effects of boundary conditions on impact energy absorptions. Shockey *et al.* [10] experimentally measured impact energy absorption under conditions in which four arms or two arms of a cruciform fabric specimen were fixed, and reported that the impact energy absorption of the specimen with the two arms fixed is higher than that with the four arms fixed. Cunniff [11] conducted impact experiments in which two edges of rectangular fabric specimens were fixed with various spacing between the two edge fixtures, and reported that the longer the spacing between the two fixtures, the greater was the impact energy absorption.

Impact energy absorptions, deceleration of an impactor and fracture mode of specimens are easily measured in the impact experiments of the high strength fiber fabrics. However, measurement of load distributions in the fabrics is very difficult. Then several computational researches were attempted to determine the load distributions in the fabrics subjected to high speed impact, and these reported the effects of boundary conditions, material properties and woven fabric structure on the impact fracture. Shockey *et al.* [12] measured elastic constants of fiber bundles and friction coefficients between the fiber bundles, and calculated impact deformations of the fabrics with two or four edges fixed. Duan *et al.* [13] also calculated effects of two and four fixed edges on the impact characteristics of the high-strength fabrics,

and the results indicated that the fabrics with two edges fixed have higher impact energy absorption characteristics compared with that having four edges fixed. Gu [14] calculated the load distributions in the fabrics fixed on a plate with a circular hole, and the calculations revealed that high stress occurs at the region which is cross-shaped with an impact point as a center of the cross.

Many researches on the impact properties of the fabrics have focused mainly on impactor penetration and ballistic energy absorption, and did not pay much attention to fracture mode and crack length in the fabrics. However, the fracture mode and the crack length are important characteristics for non-rigid airships that are impacted by high-velocity fragments from rotating propulsion units and space inflatable membrane structures impacted by high-velocity debris.

In this study, fundamental impact fracture characteristics of the coated plain-woven fabrics were measured with various fixing boundary conditions, which are very important for the ballistic impact fracture test. The effects of biaxial loads on impact fracture of the coated fabrics were evaluated with cruciform fabric specimens impacted by a high speed steel ball. Strip fabric specimens were also tested under uniaxial tension, and the effects of the specimen shape were also evaluated.

2. Experimental Procedures

2.1. Material System

The material system used in this study was coated polyarylate fiber (VECTRAN) plain weave KS26-200 (SKYPIA Co. Ltd., Japan). It was developed as an ultra-light membrane material for stratospheric airships. VECTRAN plain-weave fabric is characterized by high strength and high stiffness, and an EVAL (Kuraray Co. Ltd., Japan) film layer and polyurethane layers are applied to prevent gas leakage and mechanical damage, respectively. The area density of the coated fabric is 198 g/m^2. The line density of the warp and the weft yarns in the fabrics is 200 denier; the weave density is 13.4 yarns/cm in both directions. In this study, the x-direction and the y-direction indicate, respectively, the direction of the warp yarn and the direction perpendicular to it. Membrane specimens are cut out on the basis of the x–y coordinate system.

Reference [15] reported in-plane mechanical properties and causes of the orthotropic anisotropy of the membrane materials used in this study. The anisotropic characteristics of the materials are outlined below for the benefit of later discussion.

The warp directional tensile strength and stiffness of the membrane material KS26-200 are quite different from those in the weft direction, though the density of filament yarn and the yarn density per unit width are the same irrespective of warp or weft directions. The weft directional strength and stiffness are smaller than the warp (x-)directional ones because the crimp of the weft yarns is larger than that of the warp yarns at the crossover of these yarns in the plain weave. The dependency of strength on tensile direction is caused not only by the crimps but also by yarn misalignment and heat deterioration of the weft yarns during the coating process. In

the coating process, the fabrics were pressed with polyurethane sheets and heated to more than 150°C. The weft yarns deteriorated more than the warp yarns because the contact area of the weft yarns with heated polyurethane sheet was larger than that of warp yarns due to the larger crimp of the weft yarns.

2.2. Specimen and Loading Fixture

Impact tests with a cruciform specimen under in-plane biaxial loading were conducted. The cruciform specimen configurations used in this study are shown in Fig. 1(a). Impact tests with a strip specimen (Fig. 1(b)) under uniaxial loading were also conducted to evaluate the effects of the specimen configuration on impact fracture. The strip specimens (Fig. 1(b)) were also used to measure uniaxial strength of the fabrics.

In [15] and [16], the width of membrane specimens was defined as 30 mm for evaluating the load–strain characteristics and strength of high strength fabric materials. In this study, the width of the strip specimens and arms of the cruciform specimens was set to be 30 mm for comparison of the strength in these references and restriction of the loading fixture size. The maximum dimension of the strip and cruciform specimens was set to be 140 mm, since the size of the specimens was restricted by the size of a protective box, in which the loading fixture was installed. The width and maximum dimension of the specimens were not changed for experiments on the biaxial loading effects of impact fracture, though the width and length of membrane specimens were important factors for impact properties.

These specimens were attached to a screw-driven aluminum loading fixture as shown in Fig. 2, and subjected to tensile load before the impact test. The distance between grips was 90 mm. While the grips, which chucked the arms of the cruciform specimen, were moving by hand tightening screws, the applied loads to the specimen were being measured with 1 kN load cells (model: KM-100AK-P, Kyowa Electronic Instruments Co. Ltd., Japan) and an amplifier (model: PCD-300A, Ky-

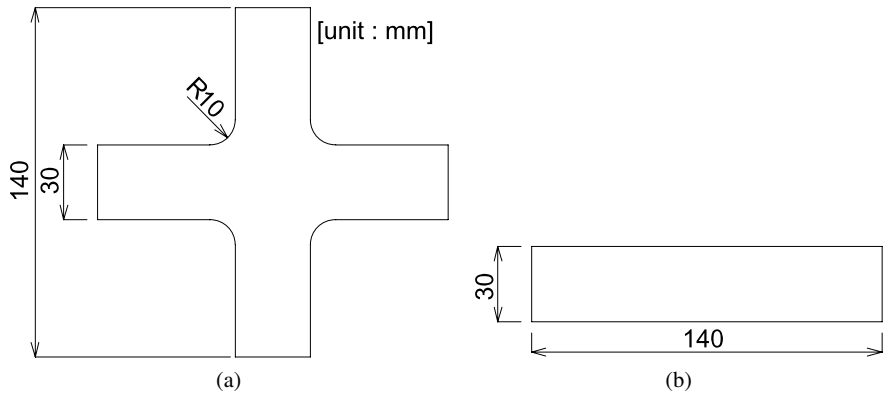

Figure 1. Specimen configuration. (a) Cruciform specimen. (b) Strip specimen.

owa Electronic Instruments Co. Ltd., Japan). Biaxial loads by hand tightening were controlled with watching the load cell output.

2.3. Impact Testing Machine

A schematic of the impact testing machine [17–19] used in this study is shown in Fig. 3. A steel ball (high carbon chrome steel SUJ-2) with diameter 5 mm and mass about 0.51 g was shot at the coated fabric specimen by a high pressure nitrogen gas. The steel ball was accelerated in a tube, passed over a laser speed sensor, and finally impacted the specimen, which was subjected to tensile load. The speed sensor was composed of two laser sensors placed at a distance 300 mm. The time interval between crossing each laser sensor was measured with a degree of accuracy of 1 μs to calculate the velocity of the steel ball. The velocity of the steel ball (impact velocity) when it impacted onto the specimen was calculated based on the time

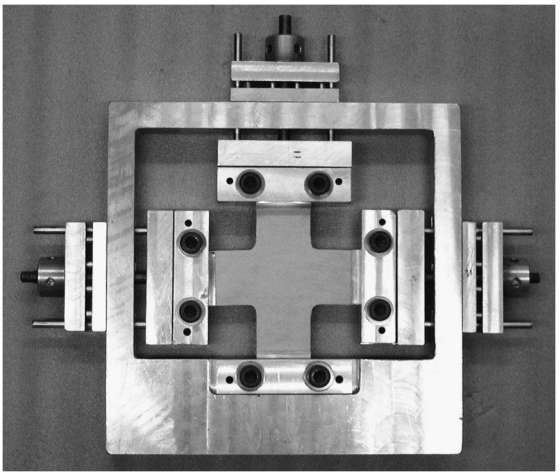

Figure 2. Loading jig and membrane specimen.

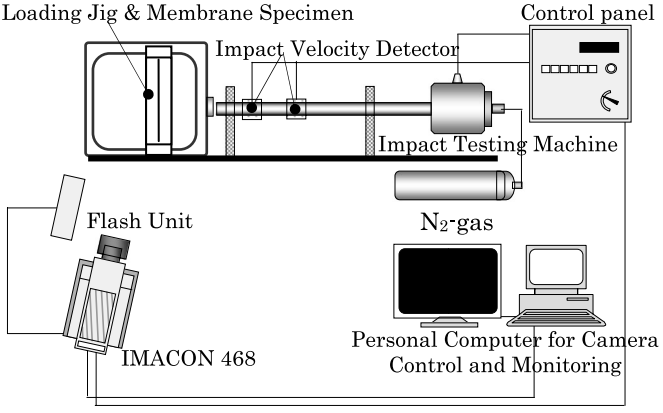

Figure 3. Schematic of impact testing system.

interval and the distance of the two laser sensors. The impact tests were conducted at atmospheric pressure and room temperature.

The impact velocity was set based on the assumption of fragment impacts to the body of stratospheric airships. In the event of breakage of propeller systems mounted on outside surface of the airships, fragments of the propellers might impact the airship envelopes. Okuyama *et al.* [20] assumed that the maximum Mach number of the blade tips allowable was 0.6 as the necessary condition to avoid a reduction in propulsive efficiency. The velocity of the steel ball impact was set as constant at 200 m/s (approximately equal to Mach 0.6) supposing the fragment impact on the membrane of the airships with the maximum Mach number. The impact velocity for each specimen was measured, and the tests with the accuracy of the impact velocity within 5% were found to be effective. Ultra-high speed photographs were taken for observation of the impact fracture. An ultra-high speed photograph system was composed of an ultra-high speed camera (model: IMACON 468, NAC Image Technology, Inc., Japan), a flash unit (model: LH-SA1, Nissin Electronic Co. Ltd., Japan), a personal computer to control the camera and an image monitor.

3. Results and Discussion

3.1. Uniaxial Strength of Strip Specimens

Uniaxial tensile strength of the strip specimens (Fig. 1(b)) was measured with using a digitized servo hydraulic material testing machine (Instron Corp., model: 4302; load capacity: 100 kN). The tensile speed was 4 mm/min. The distance between grips was 110 mm. Flat aluminum plates were inserted between the grips and the specimen. The average strengths of the three specimens in the direction of the x- and y-axis were 596 N/cm and 452 N/cm, respectively. These measured strengths approximately coincide with the experimental results with 30 mm width specimens in [15].

A measure of strength and load is frequently defined as force exerted per unit width in mechanics of woven fabrics instead of stress which is a measure of force exerted per unit area [15, 16, 21, 22], because it is difficult for non resin-impregnated woven fabrics to define the cross-sectional area. In this study, a measure of force exerted per unit width was adopted for the membrane materials KS26-200, since polyurethane in the coating sheets was scarcely impregnated into the fabrics.

3.2. Crack Width in Strip Specimens

Relationships between applied uniaxial load and crack width in the strip specimens are shown in Fig. 4, where crack width is defined as maximum length of fracture region to each direction (x- or y-direction) and includes the diameter of the hole made by the steel ball. In this paper, F_x and F_y correspond to the load parallel to

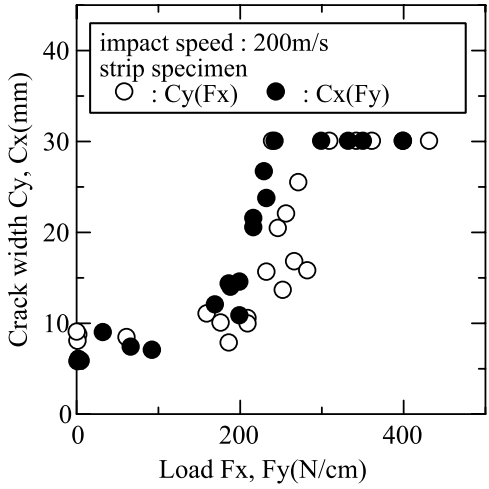

Figure 4. Relationship between applied uniaxial load and crack width in strip specimens.

the x- and the y-axis, respectively. C_x and C_y correspond to the crack width parallel to the x- and the y-axis, respectively. Figure 4 reveals the relationships between F_x and C_y and between F_y and C_x, where C_y and C_x are functions of F_x and F_y, respectively, $(C_y(F_x), C_x(F_y))$.

After the ballistic impact the crack extended through the full width of the specimen (30 mm) on condition that the uniaxial tensile load applied to x- and y-directional strip specimens was more than about 300 N/cm and about 220 N/cm, respectively. The results indicate that the crack extension through the full width of the specimen occurred with more than half of the in-plane tensile fracture load. Though the crack width is about 10 mm with the uniaxial load less than 180 N/cm, the crack width drastically increases with the uniaxial load more than 200 N/cm.

It is known that strength degradation rate of the open-hole specimens is higher than the ratio between diameter of the hole and width of the specimen [15, 21, 22]. Larger cracks under high tensile load in the impact tests were supposed to be caused not only by the impact energy consumption but also by degradation of in-plane strength due to the open hole.

The strength in the y-direction was degraded due to the thermal deterioration and the misalignment of the weft yarns, though the density of filament yarn and the yarn density per unit width are the same irrespective of warp or weft directions [15]. Shockey *et al.* reported that the impact-resistant characteristics of the fabric materials are quasi-proportional to the in-plane strength. The results of the impact tests reveal that the crack length in x-directional strip specimens, of which strength is higher than that of y-directional strip specimens, is smaller than that in y-directional strip specimens. Therefore, it should be noted that thermal deterioration of yarns in the coating process degrades not only in-plane strength but also impact properties of impact resistant structures made by high strength membrane fabrics.

3.3. Effects of Biaxial Loading on Crack Width

Relationships among F_x, F_y, C_x and C_y under biaxial loading ratios of 1 : 0, 0 : 1 and 1 : 1 are shown in Figs 5, 6 and 7, respectively. In these figures, C_y and C_x are functions of F_x and F_y in the same way as in Fig. 4 ($C_y(F_x)$, $C_x(F_y)$).

In Fig. 5, the crack width parallel to the x-axis C_x was approximately same as the diameter of the steel ball and did not extend on condition that the specimen was applied only with x-directional load F_x and the y-directional arms of the specimen

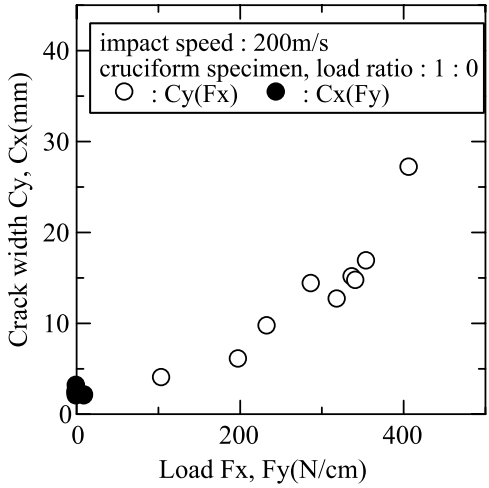

Figure 5. Relationship between applied uniaxial load and crack width in cruciform specimens ($F_x : F_y = 1 : 0$).

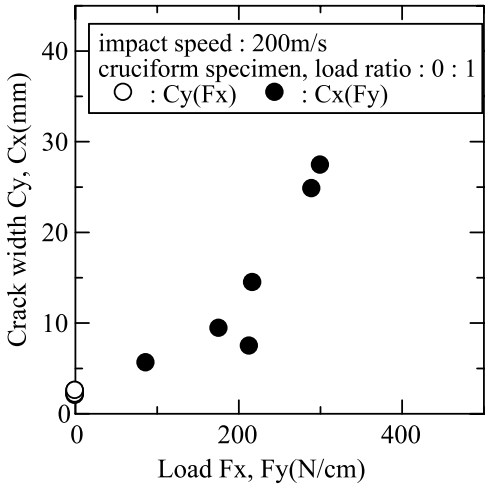

Figure 6. Relationship between applied uniaxial load and crack width in cruciform specimens ($F_x : F_y = 0 : 1$).

were fixed without tension ($F_x : F_y = 1:0$). Figure 5 also indicates that crack width parallel to the y-axis C_y, which is perpendicular to the x-axis, increases as the x-directional load F_x increases. Figure 6 also indicates similar results that only the x-directional crack width C_x perpendicular to the y-directional load F_y extends as the load F_y increases. The x-directional crack width C_x under uniaxial load F_y (Fig. 6) is larger than the y-directional crack width C_y under uniaxial load F_x (Fig. 5) due to the lower strength in the y-direction, similar to the results of the uniaxial strip specimens (Fig. 4).

When the x- and y-directional loads are equal ($F_x : F_y = 1:1$, Fig. 7), cracks in the specimen do not extend with loads less than 250 N/cm and extend only with loads more than 250 N/cm. Comparing Fig. 7 ($F_x : F_y = 1:1$) with Figs 5 ($F_x : F_y = 1:0$) and 6 ($F_x : F_y = 0:1$), the crack width with load ratio $F_x : F_y = 1:1$ drastically increases in the vicinity of 250 N/cm. In regard to the x-directional load F_x and the y-directional crack width C_y, the crack with load ratio 1 : 1 does not extend with load level in the same way as the crack with load ratio 1 : 0 extends in Fig. 5. In regard to the y-directional load F_y and the x-directional crack width C_x, the crack with load ratio 1 : 1 also does not extend at less than 250 N/cm below which the crack with load ratio 0 : 1 extends, and the crack width with load ratio 1 : 1 is almost equal to that with load ratio 0 : 1 above 250 N/cm. The y-directional crack (C_y) does not extend due to the higher x-directional strength though the x-directional crack (C_x) extends in Fig. 7.

Relationships between the crack widths and the loads in case of biaxial loading ratio $F_x : F_y = 1:0, 1:0.5, 1:1, 0.5:1$ and $0:1$ are shown in Figs 8 and 9. Figure 8 reveals the relationship between the x-directional load F_x and the y-directional crack width C_y. When the y-directional load is zero, the crack width

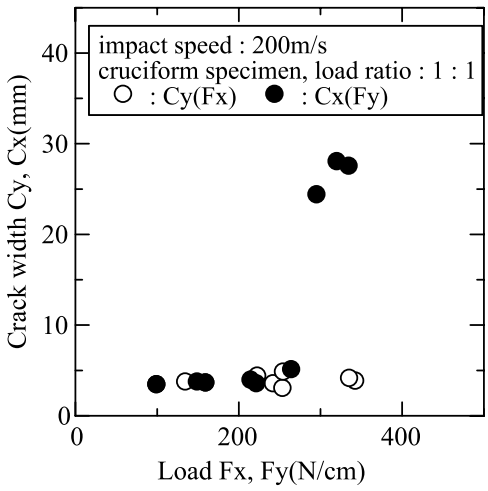

Figure 7. Relationship between applied biaxial load and crack width in cruciform specimens ($F_x : F_y = 1:1$).

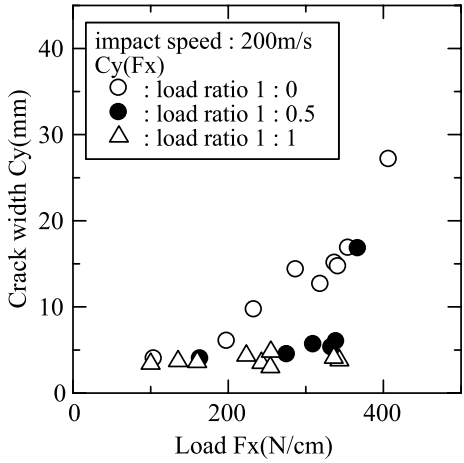

Figure 8. Relationship between x-directional load and crack width in cruciform specimens.

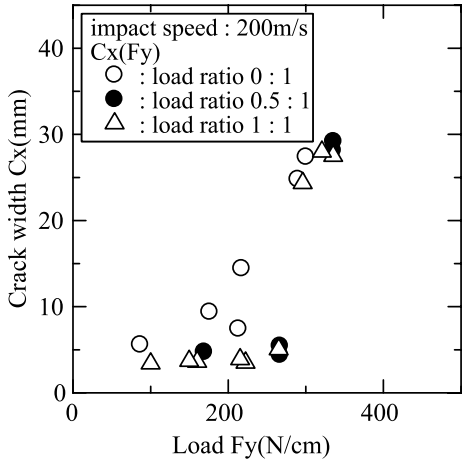

Figure 9. Relationship between y-directional load and crack width in cruciform specimens.

C_y increases with increase of the x-directional load F_x and reaches the specimen width (= 30 mm) at applied load of 400 N/cm. On the other hand, when the cruciform specimens were applied with the y-directional load F_y in addition to the x-directional load F_x (Fig. 8, $F_x : F_y = 1 : 0.5, 1 : 1$), the crack width was smaller than that under uniaxial load ($F_x : F_y = 1 : 0$). Figure 9 reveals the relationship between the y-directional load F_y and the x-directional crack width C_x. Similarly to the result in Fig. 8, the crack width of the specimen under biaxial load ($F_x : F_y = 0.5 : 1, 1 : 1$) was smaller than that under uniaxial load ($F_x : F_y = 0 : 1$) in Fig. 9.

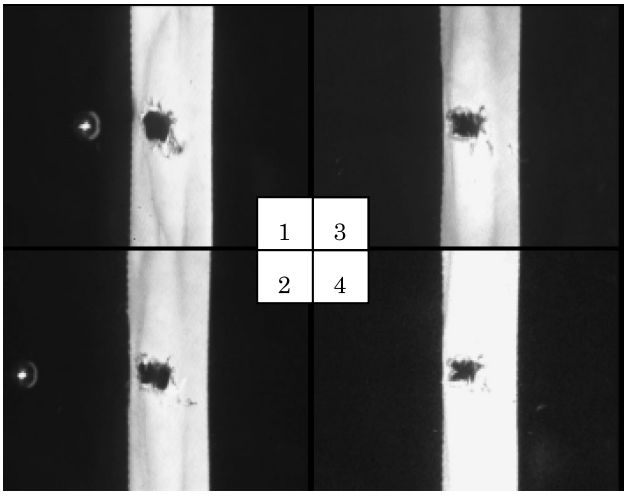

Figure 10. Ultra-high speed photograph of impact fracture of warp strip specimen under uniaxial loading ($F_x = 343$ N/cm).

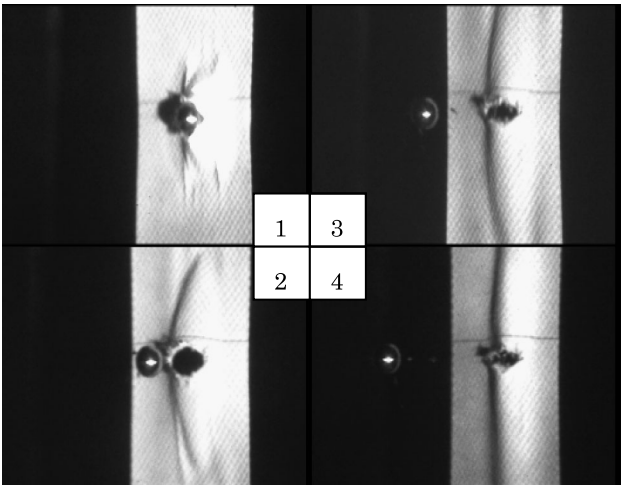

Figure 11. Ultra-high speed photograph of impact fracture of warp strip specimen under uniaxial loading ($F_y = 200$ N/cm).

3.4. Ultra-High Speed Photographs of Impact Fracture

Figures 10–14 are ultra-high speed photographs of the impact fracture. The photographs of penetration of a steel ball were taken obliquely from the backside of the specimen, where the side on which the steel ball impacts is defined as the front side. The photographs were taken four frames at 100 μs intervals with 2 μs exposure time for each figure.

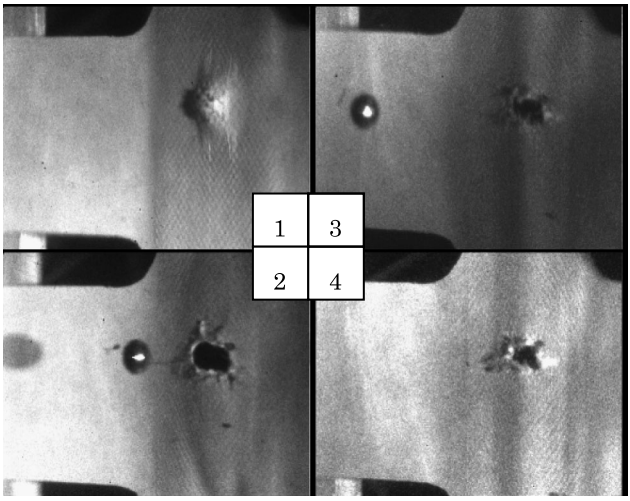

Figure 12. Ultra-high speed photograph of impact fracture of cruciform specimen under uniaxial loading ($F_x = 355$ N/cm, $F_y = 0$ N/cm).

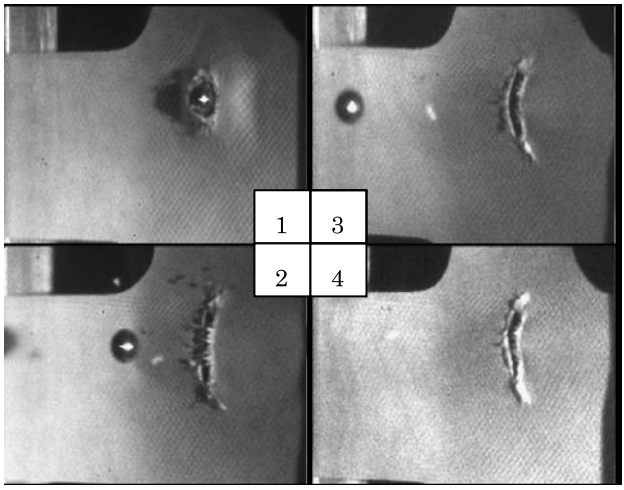

Figure 13. Ultra-high speed photograph of impact fracture of cruciform specimen under uniaxial loading ($F_x = 0$ N/cm, $F_y = 217$ N/cm).

Figures 10 and 11 are photographs of impact fracture of an x-directional strip specimen (load: 343 N/cm) and a y-directional specimen (load: 200 N/cm), respectively. Both figures indicate that a wrinkle occurred in the loading direction. In Fig. 10, only a hole in the center of the x-directional specimen is observed, but after taking the photographs in Fig. 10, the crack extended through the full width of the specimen. The crack width in the y-directional specimen in Fig. 11 did not extend through the full width. Crack extension depends on load level applied to the specimen and direction of the membrane fabric material.

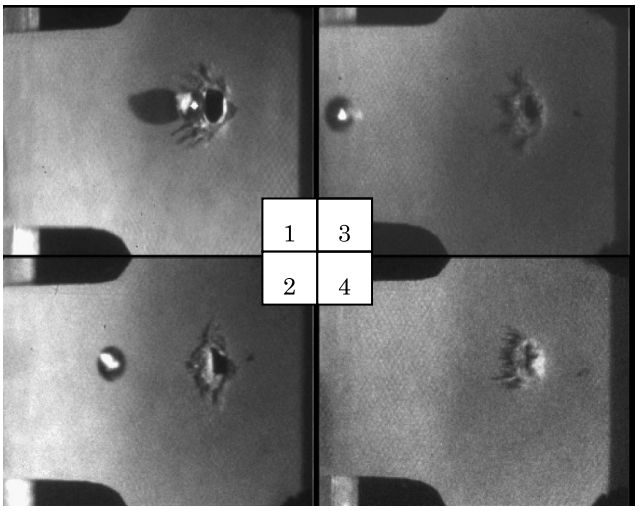

Figure 14. Ultra-high speed photograph of impact fracture of cruciform specimen under biaxial loading ($F_x = 255$ N/cm, $F_y = 265$ N/cm).

Figures 12, 13 and 14 are photographs of impact fracture under loading conditions in which (F_x, F_y) are (355 N/cm, 0 N/cm), (0 N/cm, 217 N/cm), (255 N/cm, 265 N/cm), respectively. Vertical and horizontal directions in these photographs are the x- and the y-directions, respectively. In Fig. 12 ($F_x : F_y = 1 : 0$), a wrinkle during impact occurred perpendicular to the y-direction to which tensile load did not apply. In Fig. 13 ($F_x : F_y = 0 : 1$), out-of-plane deformation near an impact point is also observed. On the other hand, out-of-plane deformation is barely observed in Fig. 14 ($F_x : F_y = 1 : 1$). It is supposed that biaxial loading ($F_x : F_y = 1 : 1$) restrained the out-of-plane deformation. Though the crack developments are not observed in Figs 12 and 14, the crack extended nearly the full arm width after taking the ultra-high speed photographs.

Comparing the strip specimens (Figs 10 and 11) and the cruciform specimens (Figs 12 and 13) under uniaxial loading, out-of-plane deformation in the center of the strip specimens is larger than that of the cruciform specimens. Displacements of two arms of the cruciform specimen perpendicular to the uniaxial load was fixed with the grips, though these two arms were not applied loading. The impacted strip specimens under uniaxial loading deformed largely due to no displacement restriction perpendicular to the uniaxial loading axis. The large deformation during the impact is supposed to cause the large crack extension in the strip specimens compared with the cruciform specimens.

The out-of-plane deformations in Figs 12 and 13 are different in spite of their being the same cruciform specimen under uniaxial loading. As the cause of the difference of the deformations it is supposed that strength and stiffness in the y-direction of the membrane materials are smaller than those in the x-direction. The impact of the steel ball onto the cruciform specimens under uniaxial loading

($F_x : F_y = 1:0$ or $0:1$, Figs 12 and 13) influences out-of-plane deformation beyond the vicinity of the impact point. However, out-of-plane deformation in cruciform specimens under biaxial loading ($F_x : F_y = 1:1$) is hardly observed in Fig. 14. The crack width in the cruciform specimens with biaxial load ratio $F_x : F_y = 1:1$ did not extend below the load level that the crack extended through the full width of the specimen with biaxial load ratio $F_x : F_y = 1:0$ or $0:1$ because the small out-of-plane deformation due to the biaxial loading ratio $F_x : F_y = 1:1$ is effective only within a limited region near the impact point. However, even though the loading ratio $F_x : F_y$ is $1:1$, the crack width extended through nearly the full arm width above the load level that crack extended through the full width of the specimen with biaxial load ratio $F_x : F_y = 0:1$. Diameter of the steel ball 5 mm is about 17% of the arm width of the cruciform specimens (30 mm). Researches described in [15, 21] and [22] reported that the decreasing rate of tensile strength of fabric membrane materials with an open hole is more than the ratio of the open hole against specimen width. In Fig. 9, the applied tensile load that the crack width extends nearly the whole arm width after impact (250 N/cm) is about 55% load of the y-directional strength. It is supposed that the crack extension reach the full arm width at higher biaxial loading due to degradation of the in-plane strength after the formation of the impact hole.

3.5. Effect of Specimen Configuration and Dimension on Crack Width After Impact

Figures 15 and 16 reveal the y-directional crack width C_y of the cruciform and the strip specimens with the applied x-directional uniaxial load ($F_y = 0$), and the x-directional crack width C_x of the cruciform and the strip specimens with the applied y-directional uniaxial load ($F_x = 0$), respectively. Even though both cruciform and

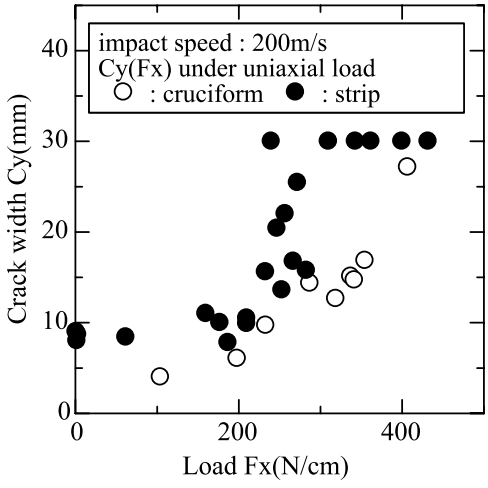

Figure 15. Relationship between applied uniaxial load and crack width in strip and cruciform specimens ($F_x : F_y = 1:0$).

strip specimens were subjected to an equivalent uniaxial load, the crack width in the cruciform specimens is smaller than that in the strip specimens. The x-directional load under which the crack width reaches the specimen width (= 30 mm) of the cruciform specimen is 30% larger than that of the strip specimen in Fig. 15. A cause of the small crack width in the cruciform specimens compared with the strip specimens is supposed to be the fixing condition: the y-directional arms of the cruciform specimen were fixed by the grips of the fixture frame without mechanical tension load.

Research on in-plane tensile strength [15] reported little effect of the specimen configuration difference (strip/cruciform) on tensile strength with an open hole. However, as mentioned above, the specimen configuration has a large effect on the impact fracture properties of the impact tests.

Shockey *et al.* [10] conducted impact experiments on fabric materials and reported that the fabric specimens fixed at two edges absorbed larger kinetic energy of a projectile than those fixed at all four edges. Though Shockey *et al.* did not describe the damage state of the fabrics after impact, it is supposed that the specimens with their two edges fixed that absorbed the larger ballistic energy have more severe breakage compared with the specimens with their four edges fixed. Numerical calculations conducted by Duan *et al.* [13] indicated that fabrics with two edges fixed absorbed more ballistic energy compared with the fabrics with four edges fixed. Though ballistic energy loss after the impact was not measured in their study, it is supposed that ballistic energy absorption of the four arms fixed cruciform specimens is larger than that of the two edges fixed strip specimens on the assumption that the greatest part of the ballistic energy loss is consumed for the breakage of the membrane fabrics. Though a tensile load was not applied to the membrane fabrics

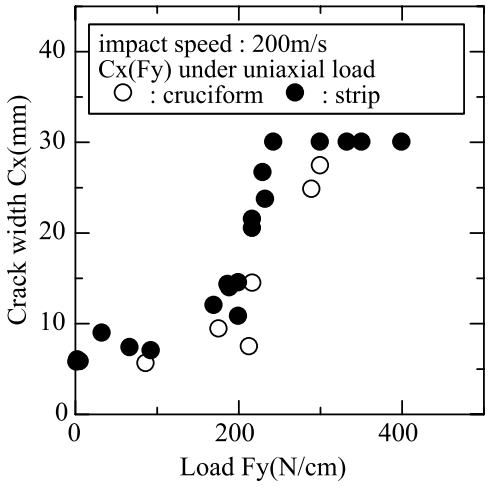

Figure 16. Relationship between applied uniaxial load and crack width in strip and cruciform specimens ($F_x : F_y = 0 : 1$).

in the researches by Shockey *et al.* and Duan *et al.*, their results showed the same tendencies as in this study.

The results of the impact tests are known to be sensitive to specimen dimensions. Impact characteristics measured with small specimens is particularly affected by reflection of elastic waves at the support boundaries and the specimen edges. The effect of the elastic wave reflections on the results in this study could be examined by using the approximated speeds of in-plane elastic wave (longitudinal wave) and out-of-plane elastic wave (transverse wave) with no mechanical loads. The speeds of in-plane elastic wave (longitudinal wave) and out-of-plane elastic wave (transverse wave) are approximated to be less than 2000 m/s and less than 500 m/s, respectively, in Appendix A.

The results of the impact tests indicate that the steel ball penetrated the membrane specimen within 100 μs, which was the time interval between frames of the ultra-high speed photographs. Reflection of the in-plane waves significantly affected the impact fracture of the cruciform specimens in this study, since the in-plane elastic wave propagation during 100 μs was more than 200 mm, which was more than the length between impact point and grip edges (45 mm). Reflection of the out-of-plane waves has little influence on the initial stage of the impact fracture of the cruciform specimens, because the out-of-plane elastic wave propagation during 100 μs was less than 50 mm. However, the reflection of the out-of-plane waves might affect the later stage of the impact fracture. Reflections of both in-plane and out-of-plane wave affected the impact fracture of the strip specimens due to the short distance between the impact point and free edges of the strip specimens. The large effect of the in-plane and out-of-plane wave reflections was supposed to be one of the causes of larger crack propagation in the strip specimens than the cruciform specimens.

The length of the specimens used in this study is not sufficiently long to avoid influence of the elastic wave reflections. The effects of the elastic wave reflections on the impact fractures could not be evaluated because impact tests with variation of specimen length were not conducted. In future work, it is planned to investigate the influence of elastic wave reflection on impact fractures. For impact tests without effect of elastic wave reflections, the distance between impact point and boundaries needs to be sufficiently long when using a large specimen. However, it is difficult to conduct the impact tests with a sufficiently large specimen because the in-plane elastic wave speed of high strength fabric materials is very high. In addition to the experimental study, a numerical study such as finite element analysis is necessary to investigate the effect of the elastic wave reflections on impact fractures of high strength fabric materials.

4. Conclusion

In this paper, high speed impact tests on a cruciform and on a strip membrane fabric specimen were conducted to clarify the effects of biaxial loading on impact

fractures of the coated fabric materials. Results of the impact experiments indicate that the crack width in the cruciform specimens under biaxial loading does not extend less than that under uniaxial loading when the applied loads are less than 60% of the uniaxial tensile strength. However, when the applied load level is above 60%, the crack development in the cruciform specimens under the biaxial loading is almost the same as that under uniaxial loading. Experimental results of the strip specimens compared with the cruciform specimens reveal that crack width in the strip specimens is larger than that in the cruciform specimens due to the difference in the fixing conditions.

Acknowledgements

The authors wish to acknowledge Ken-ich Ishida (former graduate student, Takushoku University) for assistance in impact testing, and SKYPIA Co. Ltd. for providing the membrane materials.

References

1. K. Eguchi, Y. Yokomaku, M. Mori, N. Yamauchi, M. Maruhashi, N. Tabo, K. Oogaki, J. Kimura and H. Nakamura, Feasibility study program on stratospheric platform airship technology in Japan, in: *AIAA Paper 99-3912, Intl Balloon Technol. Conf.*, Norfolk, VA, USA (1999).
2. S. Takeda and T. A. Kohno, Stratospheric platform airship system, *J. Japan Soc. Aeronaut. Space Sci.* **52**, 22–29 (2004) (in Japanese).
3. R. Mollerick, *New Millennium Inflatable Structures Technology*, NASA TM-112828 (1997).
4. A. T. Weaver, in: *Lightweight Engine Containment: An Assessment of Technology for Turbojet Engine Rotor Failures*, NASA CP-2017, pp. 235–245 (1977).
5. D. A. Shockey, J. W. Simons and D. C. Elrich, *Improved Barriers to Turbine Engine Fragments: Interim Report I.* United States Department of Transportation Federal Aviation Administration Report DOT/FAA/AR-99/8, I (1999).
6. A. Fujiwara and H. Yano, The asteroidal sampling system on board the Hayabusa spacecraft, *J. Japan Soc. Aeronaut. Space Sci.* **53**, 264–271 (2005) (in Japanese).
7. D. Cadogan, C. Sandy and M. Grahne, Development and evaluation of the Mars Pathfinder inflatable airbag landing system, *Acta Astronautica* **50**, 633–640 (2002).
8. J. Stein and C. Sandy, Recent developments in inflatable airbag impact attenuation systems for Mars exploration, in: *AIAA Paper, 2003–1900, 44th AIAA/ASME/ASCE/AHS/ASC, Struct. Struct. Dynamics Mater. Conf.*, Norfolk, VA, USA (2003).
9. D. S. Adams, Mars exploration rover airbag landing loads testing and analysis, in: *AIAA Paper 2004-1795, 45th AIAA/ASME/ASCE/AHS/ASC Struct. Struct. Dynamics Mater. Conf.*, Palm Springs, CA, USA (2004).
10. D. A. Shockey, J. W. Simons and D. C. Elrich, *Improved Barriers to Turbine Engine Fragments: Interim Report II.* United States Department of Transportation Federal Aviation Administration Report, DOT/FAA/AR-99/8, II (1999).
11. P. M. Cunniff, An analysis of the system effects in woven fabrics under ballistic impact, *Textile Res. J.* **62**, 495–509 (1992).

12. D. A. Shockey, D. C. Elrich and J. W. Simons, *Improved Barriers to Turbine Engine Fragments: Interim Report III.* United States Department of Transportation Federal Aviation Administration Report, DOT/FAA/AR-99/8, III (2001).
13. Y. Duan, M. Keefe, T. A. Bogetti and B. A. Cheeseman, Modeling the role of friction during ballistic impact of a high-strength plain-weave fabric, *Compos. Struct.* **68**, 331–337 (2005).
14. B. Gu, Ballistic penetration of conically cylindrical steel projectile into plain-woven fabric target — a finite element simulation, *J. Compos. Mater.* **38**, 2049–2074 (2004).
15. H. Kumazawa, I. Susuki, T. Morita and T. Kuwabara, Mechanical properties of coated plain weave fabrics under biaxial loads, *Trans. Japan Soc. Aeronaut. Space Sci.* **48**, 117–123 (2005).
16. S. Maekawa, K. Tanaka and Y. Hamaguch, *Study on the Residual Strength and the Test Method for Envelope Materials after Low Altitude Stationary Flight Test*, JAXA Research and Development Report, JAXA-RR-06-030(2007) (in Japanese).
17. O. Hasegawa, T. Okubo, S. Yamagata, S. and H. Kasano, Application of ultra-high speed photography to analytical modeling of impact perforation of polymer and ceramic materials, in: *24th Intl Congr. High-Speed Photogr. Photon*, Sendai, Miyagi, Japan, pp. 1–7 (SPIE Proc.) 4183 (2001).
18. H. Kasano, S. Yamagata and O. Hasegawa, Ballistic impact properties and behavior of structural ceramics at high temperature, in: *Proc. Tenth US-Japan Conf. Compos. Mater.*, Stanford, CA, USA, pp. 581–587 (2002).
19. H. Kasano, O. Hasegawa and N. Nanjyo, Ballistic impact properties of polymer and polymer matrix composites, in: *Proc. Eleventh US-Japan Conf. Compos. Mater.*, Yonezawa, Yamagata, Japan, pp. 3.1–3.4 (2004).
20. M. Okuyama, M. Shibata, A. Yokokawa and K. Kimura, *Study of Propulsion Performance and Propeller Characteristics for Stratospheric Platform Airship*, JAXA Research and Development Report, JAXA-RR-05-056 (2006) (in Japanese).
21. H. Minami, Strength of coated fabrics with crack, *J. Japan Soc. Compos. Mater.* **4**, 81–87 (in Japanese) (1978).
22. H. Minami, H. Yoyoda and W. Yung, Crack-tear-strength properties of coated plain-weave fabrics, *J. Soc. Mater. Sci. Japan* **41**, 913–919 (in Japanese) (1992).
23. J. C. Smith, J. M. Blandford and H. F. Schiefer, Stress–strain relationships in yarns subjected to rapid impact loading. Part VI: Velocities of strain waves resulting from impact, *Textile Res. J.* **30**, 752–760 (1960).
24. T. Kinrai, A. Hojo, A. Chatani, S. Shintaku and I. Arai, An impact tensile testing apparatus for yarn and mechanical properties of aramid fiber yarn at high strain rate, in: *Proc. 33rd Japan Congr. Mater. Res.*, Kyoto, Japan, pp. 87–91 (1990).

Appendix

A. Elastic wave velocity

The elastic wave velocity in membrane fabrics was approximately estimated by using an analytical model originally developed for a single yarn which was impacted perpendicular to the yarn and was not subjected to tensile load [23]. In the approximation of in-plane elastic wave (longitudinal wave) and out-of-plane elastic wave (transverse wave) velocities, deformation of the fabric membrane materials were assumed to be two dimensional.

Smith *et al.* [23] derived the velocity of in-plane elastic wave and out-of-plane elastic wave in a single yarn under the assumption that a projectile is impacted

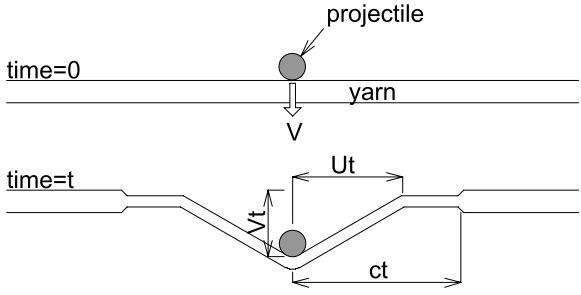

Figure A.1. A projectile transversely impacts on a long straight yarn at a constant velocity.

perpendicular to the yarn at time 0 s with velocity V m/s and velocity is constant (independent of time t in seconds) as shown in Fig. A.1. The in-plane elastic wave velocity c (m/s) and the out-of-plane elastic wave velocity U (m/s) are expressed as follows,

$$c = \sqrt{\frac{E}{\rho}}, \tag{A.1}$$

$$U = c\sqrt{\frac{\varepsilon}{1+\varepsilon}}, \tag{A.2}$$

where E is the elastic constant of the single yarn, ρ is the yarn density, and ε is the tensile strain behind the in-plane elastic wave front. The tensile strain ε is solved from the following equation:

$$2\varepsilon\sqrt{\varepsilon(1+\varepsilon)} - \varepsilon^2 = \frac{\rho V^2}{E}. \tag{A.3}$$

Generally, the out-of-plane elastic wave velocity U is smaller than the in-plane elastic wave velocity c and larger than the projectile velocity V.

Warp and weft directional elastic constants are 12.8 kN/cm and 8.07 kN/cm, respectively, which are calculated by linear approximation of static load–strain curves in [15]. In-plane elastic wave velocities c in the direction of warp and weft are estimated to be 2538 m/s and 2018 m/s, respectively, which are derived from (A.1) under the condition of impact velocity $V = 200$ m/s. Out-of-plain wave velocities U in the direction of warp and weft are estimated to be 374 m/s and 346 m/s, respectively, which is derived from (A.2) and (A.3). Non-linear (A.3) was solved using MATLAB Ver.6.5 (MathWorks Inc.).

Reference [24] reported that the elastic constants of high strength fibers increase under high strain rate. Even though dynamic elastic constants are assumed to be five times larger than static ones, out-of-plain wave velocities U in the direction of warp and weft are estimated to be 489 m/s and 453 m/s, respectively, which are not more than 1.5 times of those with static elastic constants.